IEEE Photonics Journal
An IEEE Photonics Society Publication

Open Access

Emission Characteristics of a 1.5-μm All-Semiconductor Tapered Master Oscillator Power Amplifier

Volume 7, Number 2, April 2015

M. Vilera
A. Pérez-Serrano
J. M. G. Tijero
I. Esquivias

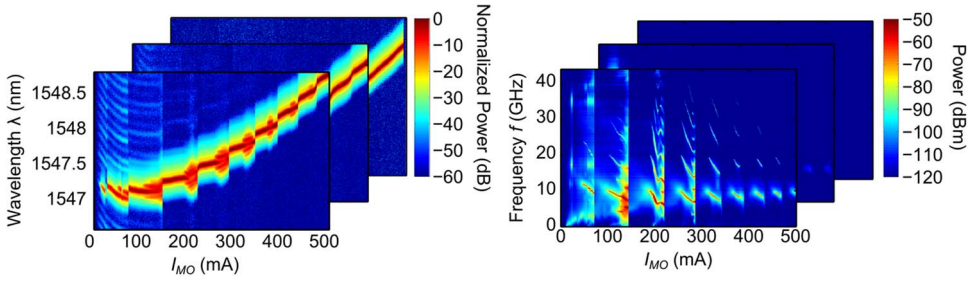

DOI: 10.1109/JPHOT.2015.2402597
1943-0655 © 2015 IEEE

Emission Characteristics of a 1.5-μm All-Semiconductor Tapered Master Oscillator Power Amplifier

M. Vilera, A. Pérez-Serrano, J. M. G. Tijero, and I. Esquivias

CEMDATIC-E.T.S.I. Telecomunicación, Universidad Politécnica de Madrid, 28040 Madrid, Spain

DOI: 10.1109/JPHOT.2015.2402597

Manuscript received December 28, 2014; revised February 5, 2015; accepted February 6, 2015. Date of publication February 10, 2015; date of current version February 25, 2015. This work was supported by the European Commission through the project BRITESPACE under Grant 313200, by the Ministerio de Economía y Competitividad of Spain under project RANGER (TEC2012-38864-C03-02), and by the Comunidad de Madrid under program SINFOTON-CM (S2013/MIT-2790). Corresponding author: M. Vilera (e-mail: mf.vilera@upm.es).

Abstract: We present experimental results on the emission characteristics of a 1.5-μm distributed feedback (DFB) tapered master oscillator power amplifier (MOPA) in a wide range of steady-state injection conditions, showing different dynamical behaviors. A detailed analysis of the optical and radio-frequency spectra has allowed the identification of three different emission regimes: i) stable amplified DFB emission, but with wavelength jumps when sweeping the injection currents; ii) multimode Fabry–Perot (FP) operation of the complete MOPA cavity; and iii) self-pulsed operation at frequencies between 5 and 8 GHz. The quasi-periodic occurrence of these emission regimes as a function of the injected currents is interpreted in terms of a thermally tuned competition between the modes of the master oscillator and the compound cavity modes. The physical origin of the wavelength jumps and of the alternation between regimes is discussed.

Index Terms: High power semiconductor lasers, master oscillator power amplifier, multimode dynamics.

1. Introduction

Directly modulated high brightness semiconductor lasers are required for many applications. In particular, these devices modulated at high speed are attractive sources for applications such as LIDAR, free space optical communications, and laser projection displays. The Master Oscillator Power Amplifier (MOPA) architecture is a suitable choice for these applications since large changes in the output power can be obtained at high frequencies with a relatively small current excursion in the Master Oscillator (MO). Monolithically integrated MOPAs are multiple section devices usually composed of an index guided single lateral mode waveguide section acting as MO, and a Power Amplifier (PA) section [1]–[5]. The MO is either a Distributed Bragg Reflector (DBR) or a Distributed Feedback (DFB) laser, while the PA is a gain guided tapered section with antireflection coated output facet providing high power and good beam quality.

Over the past few years, a good deal of progress has been achieved in the development of monolithically integrated MOPA sources. Power of 12 W in the Continuous-Wave (CW) regime has been demonstrated at 1064 nm, has pulse generation with 42 W peak power and 84 ps pulse width [1]. At an eye-safe wavelength close to 1.5 μm, we have demonstrated the

generation of 100 ps wide pulses with peak power up to 2.7 W at 1 GHz by Gain-Switching the MO section of commercial devices which achieve 1.6 W output power under CW conditions [2].

In a MOPA working under ideal conditions, the single lateral and longitudinal mode generated by the MO is launched into the PA section where it undergoes free diffraction and amplification while keeping its initial beam quality. However, the residual reflectance of the amplifier front facet induces emission instabilities attributed to the coupling of the oscillator modes and the modes of the full MOPA cavity, even when both sections are driven in CW conditions [3]. One of the manifestations of these instabilities is the appearance of ripples in the Power-Current (P-I) characteristics which have been attributed to longitudinal mode hopping and multimode effects [5]. These effects result also in self-pulsations due to the mode beating at the frequency of the spacing between neighboring modes [2]. The instabilities also manifest as strong self-pulsations at a few GHz attributed to undamped Relaxation Oscillations (ROs) [3].

The physical mechanisms involved in the complex spatio-temporal dynamics shown by high power MOPAs have been investigated by means of different simulation models that include coupled cavity effects [4]. These models have successfully reproduced the experimentally observed phenomena when properly addressing thermal effects [5]. The observed periodic mode hopping and the associated ripples in the P-I curve are attributed to the effect on the coupled cavity modal dynamics of the thermally induced refractive index changes in both sections, mediated by self- and cross-heating effects [8]. Similar thermal drifts and multimode competition mechanisms have been invoked to explain the dynamics of integrated ring lasers [6], and passively mode-locked lasers [7].

In previous works [2], [9], we have also reported a very rich spectral dynamics with different emission regimes and a quasi-periodic alternation between them as a function of the CW currents in both sections. All these CW effects are expected to have a substantial impact on the operation of MOPAs in direct modulation and therefore it is of primary interest the detailed characterization and understanding of the performance of these devices under CW injection conditions. In this paper we perform a systematic experimental investigation of the emission characteristics of integrated MOPAs as a function of the CW injection conditions and provide a qualitative physical explanation of the alternation between the different emission regimes. We show injection conditions in which CW emission is stable, i.e., it is not affected by compound cavity effects. Moreover, we provide a deeper insight into the longitudinal mode hopping effects on the device performance under specific injection conditions. The paper is organized as follows: In Section 2 details of the device, the experimental techniques used in its characterization and the measurement setup are presented. Section 3 is devoted to the description of the experimental results including the P-I characteristics and the optical and Radio-Frequency (RF) spectra, and to the definition of the observed emission regimes. In Section 4 the transitions between the regimes are analyzed and a qualitative explanation of the observed dynamics is discussed. Finally, a summary of the conclusions is given in Section 5.

2. Experimental Setup

The investigated devices are commercial MOPAs working at 1547 nm (QPC 4715-0000). Three devices were measured showing similar emission characteristics. All the results shown in this paper correspond to the same device (#1), unless it is explicitly indicated that they correspond to the second device (#2), which was used for detailed measurements after accidental failure of device #1. The total device length is $\sim$2.5 mm, the DFB section is $\sim$0.9 mm, and the output facet width is $\sim$250 μm. A photograph of one of the devices is shown in Fig. 1(a). The devices are p-up mounted onto a C-mount. All the measurements were performed at 25 $^{\circ}$C. For measuring the total power, a broad area thermal detector (Gentec UP19K-30H-H5) was placed close to the output facet and was slightly tilted to avoid feedback effects.

The experimental setup shown in Fig. 1(b) was used to record the optical and RF spectra of the devices. Each section was separately driven in CW. A fraction of the output power (around 0.1%) was collected using a lensed fiber. An optical isolator was used to avoid reflections. The

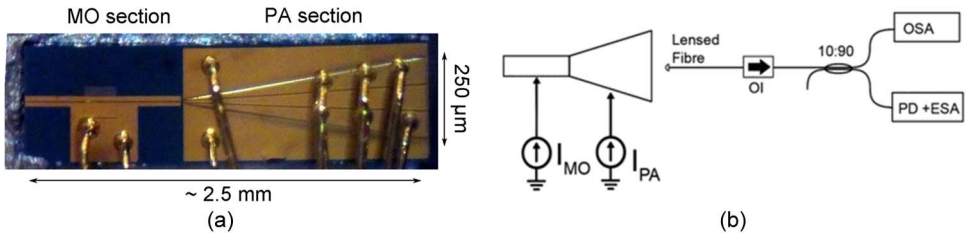

Fig. 1. (a) MOPA device. (b) Experimental setup for acquisition of the optical and RF spectra: optical isolator (OI), optical spectrum analyzer (OSA), photodetector (PD), and electrical spectrum analyzer (ESA).

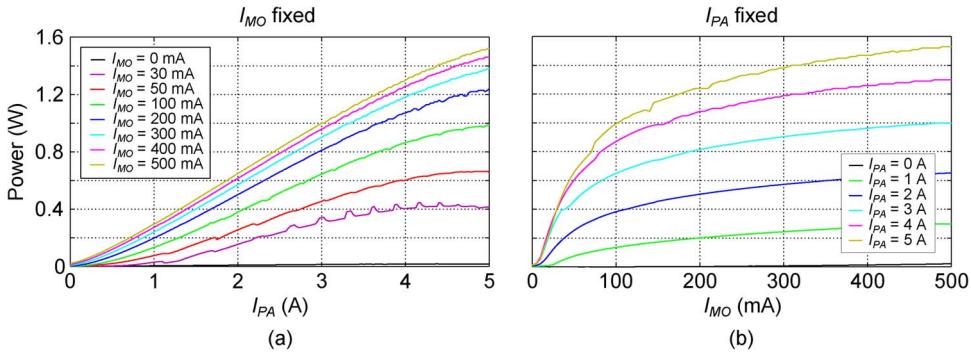

Fig. 2. P-Current characteristics. (a) For different fixed values of I_{MO} while varying I_{PA}. $\Delta I_{PA} = 0.025$ A. (b) For different fixed values of I_{PA} while varying I_{MO}. $\Delta I_{MO} = 1$ mA.

optical signal was splitted into two branches: one directed to an Optical Spectrum Analyzer (ANDO AQ6315) with a resolution $\Delta\lambda = 0.05$ nm, and the other one to a 45 GHz photodiode (New focus 1014) and a 44 GHz Electrical Spectrum Analyzer (Agilent E4446A). It was checked that RF and optical measurements were not affected by the position of the lensed fiber, and that they were reproducible. No signs of hysteresis were found when recording the PI-characteristics and the optical and RF spectra while sweeping the currents upwards and downwards.

3. Results

Fig. 2(a) and (b) shows the output power as a function of the PA (MO) section current I_{PA} (I_{MO}) while keeping constant the MO (PA) section current. The acquisition time for each measurement was 500 ms. The output power increases almost linearly as a function of I_{PA}, at high values of I_{MO}, while at low values of I_{MO} it shows a clear thermal rollover. This is due to the balance between the electrical power supplied to the device and the optical output power: At high I_{MO} the output power is higher than at low I_{MO}, hence the dissipated electrical power is lower and the chip temperature and therefore the thermal rollover are reduced. The P-I_{MO} characteristics in Fig. 2(b) show a DFB threshold current $\sim$30 mA and subsequent gain saturation when increasing I_{MO} at low I_{PA} (1 A). At higher I_{PA}, the threshold current decreases and the saturation power increases.

The most relevant feature in Fig. 2(a) is the appearance of ripples similar to those previously reported in 1060 nm MOPAs [5] and DBR tapered lasers [10]. At low I_{MO}, they are clearly visible, whereas at higher values of I_{MO} they are only apparent in the derivatives of the P-I curves (not shown). These ripples are related to transitions between different emission regimes [9], which will be later described in detail.

The optical and RF spectra reveal a very complex dynamics, with different emission regimes depending on the two parameters characterizing the CW injection conditions, namely, I_{MO} and I_{PA}. In order to illustrate these emission regimens as well as the transitions between them we

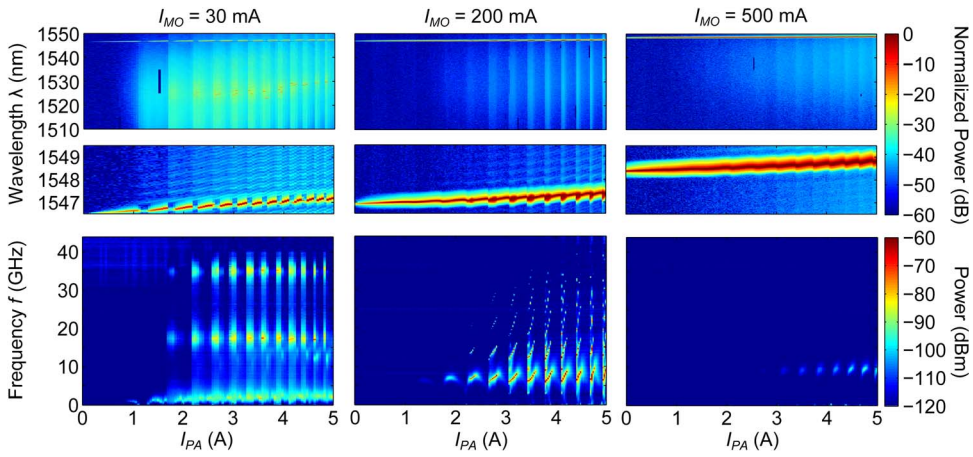

Fig. 3. Optical spectra (upper and central rows) and RF spectra (lower row) while varying I_{PA} for $I_{MO} = 30$, 200, and 500 mA corresponding to each column. $\Delta I_{PA} = 0.025$ A.

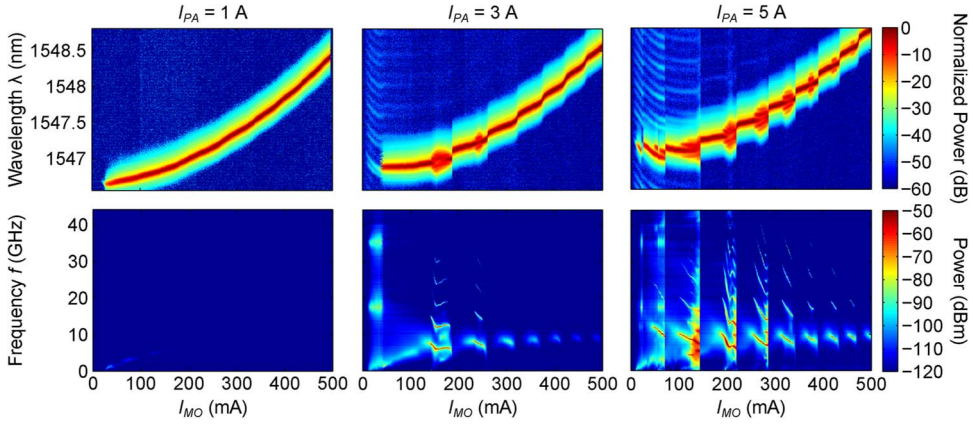

Fig. 4. Optical spectra (upper row) and RF spectra (lower row) while varying I_{MO} for $I_{PA} = 1$, 3, and 5 A corresponding to each column. $\Delta I_{MO} = 1$ mA.

have selected specific injection conditions and analyzed the corresponding optical and RF spectra. Fig. 3 shows the evolution of these spectra as a function of I_{PA} for $I_{MO} = 30$, 200, and 500 mA. The optical spectra (upper rows) are plotted in the ranges $1510 < \lambda < 1550$ nm and $1546.5 < \lambda < 1549.5$ nm where they show non-vanishing values. Each vertical line corresponds to a single spectrum normalized to the maximum value in the whole plot. The corresponding RF spectra recorded under the same conditions are plotted in the lower row. The main features of Fig. 3 are the quasi-periodic jumps and the red shift of the optical spectra correlated with a quasi-periodic evolution of the RF spectra as a function of I_{PA}. These phenomena will be analyzed in the next section.

In a similar way, Fig. 4 shows the evolution of the optical and RF spectra as a function of I_{MO} for $I_{PA} = 1, 3$, and 5 A. Under these conditions no significant power was emitted in the range of $1520 < \lambda < 1530$ nm, and therefore, the spectra in this region have not been plotted. While at $I_{PA} = 1$ A the emission is single frequency for the whole range of I_{MO}, at higher I_{PA} the evolution of the optical spectra show a quasi-periodic alternation between three emission regimes, each one characterized by specific features of the optical and RF spectra. In the following we will first describe the characteristics defining each regimes and then, in next section, we will analyze the transitions between them providing a qualitative interpretation.

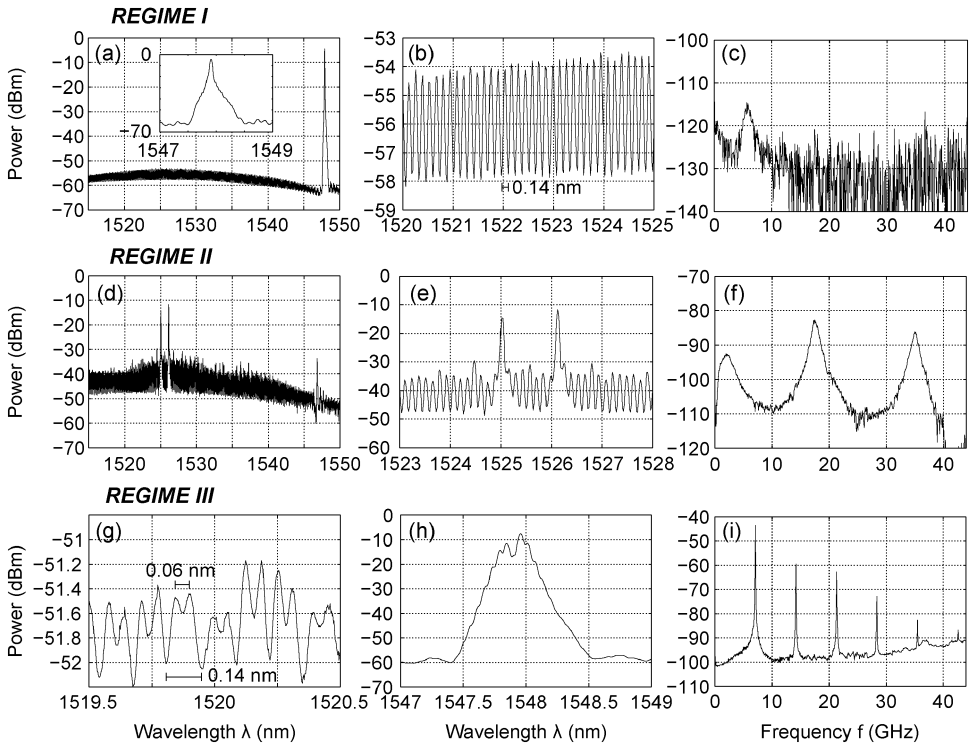

Fig. 5. Regime I: (a) Optical spectrum (inset: centered in the λ_{Bragg}), (b) optical spectrum around $\lambda \sim 1522$ nm, and (c) RF spectrum. $I_{MO} = 315$ mA and $I_{PA} = 4$ A (device #2). Regime II: (d) Optical spectrum, (e) optical spectrum around $\lambda \sim 1525$ nm, and (f) RF spectrum. $I_{MO} = 30$ mA and $I_{PA} = 3.05$ A (device #1). Regime III: (g) Optical spectrum around $\lambda \sim 1520$ nm, (h) optical spectrum around $\lambda \sim 1548$ nm, and (i) RF spectrum. $I_{MO} = 330$ mA and $I_{PA} = 4$ A (device #2).

3.1. Regime I. Amplified DFB Operation

We define as Regime I the operation of the MOPA, consisting in the single frequency emission of the DFB section with a high Side Mode Suppression Ratio (SMSR) and subsequent amplification in the PA section without spectral changes. We consider the emission to be in this regime when the SMSR is higher than 40 dB and there are no peaks above -100 dBm in the RF spectra. The emission wavelength, close to the Bragg grating wavelength (λ_{Bragg}), ranges between 1546 and 1549 nm, depending on the injection conditions.

This regime appears at low I_{PA} for the whole range of I_{MO} (see Fig. 4, $I_{PA} = 1$ A), at high I_{MO} current for the whole range of I_{PA} (see Fig. 3, $I_{MO} = 500$ mA), and in quasi-periodic regions when sweeping both currents. Fig. 5(a)–(c) illustrate this regime for high injection of the PA section. The complete spectrum has been plotted in Fig. 5(a). It includes a broad Amplified Spontaneous Emission (ASE) spectrum with its maximum around 1530 nm together with the laser peak determined by the DFB. The peak position at around $\lambda = 1547$ nm and a SMSR ~ 50 dB are shown in the inset. Fig. 5(b) shows a detail of the ASE spectrum. The modal separation ~ 0.14 nm corresponds to the Free Spectral Range (FSR) of the complete cavity (2.5 mm). Finally, Fig. 5(c) shows the corresponding flat RF spectrum with only a weak broad peak at ~ 5.6 GHz, attributed to the ROs.

3.2. Regime II. Multimode Fabry-Perot Operation

This regime is characterized by rapidly variable optical spectra dominated by the longitudinal Fabry–Perot (FP) modes of the complete cavity at the maximum of the gain spectrum, and a weak RF peak at 18 GHz (and its harmonic at 36 GHz), the frequency corresponding to the modal separation of the FP peaks (0.14 nm).

This regime appears only for low injection of the MO section and it alternates with Regime I (see Fig. 3, $I_{MO} = 30$ mA). Fig. 5(d)–(f) illustrate this case. The emission around $\lambda = 1547$ nm is reduced below -30 dB, while several peaks appear around the maximum of the gain spectrum as in FP lasers [see Fig. 5(d)]. As a result of the fast dynamics of mode hopping, the recorded optical spectra are not reproducible. They show one, two [see Fig. 5(e)], or more predominant modes. The beating of these FP modes produces the 18 GHz and its higher order harmonics. A Relative Intensity Noise (RIN) peak at a RO frequency of 2–3 GHz is also apparent in this spectrum [see Fig. 5(f)].

3.3. Regime III. Self-Pulsed Operation

Regime III is characterized by multi-peak optical spectra close to the λ_{Bragg} together with strong RF multiple peaks, or broad RF spectra, with the strongest peak at frequencies between 5 and 8 GHz, depending on the injection conditions. At some specific conditions, the RF spectra broaden revealing a behavior close to chaos. This regime appears only for short current ranges, and alternates quasi-periodically with regime I when sweeping the injected currents (see Fig. 3, $I_{MO} = 200$ mA and Fig. 4, $I_{PA} = 3$ and 5 A). Fig. 5(g)–(i) show an example of this regime. In this case the self-pulsation results in the strong RF peak at $\sim$7 GHz with five higher order harmonics [see Fig. 5(i)]. In the optical spectra, the separation between the multiple peaks at the laser emission [see Fig. 5(h)] ranges between 0.05 nm and 0.07 nm, depending on the injection conditions and corresponds to the self-pulsation frequency. Same peak separation is observed in the short wavelength region [see Fig. 5(g)] as a modulation of the distance between the FP modes.

4. Discussion

Each of the three emission regimes observed in this work has been previously reported in different types of multiple-section laser devices. While a stable Regime I is the expected behavior of an ideal MOPA, the residual front facet reflectivity allows the coupling of the two resonant cavities, giving rise either to the lasing of the FP modes of the complete cavity, regime II [5] or to an active feedback to the MO which induces the self-pulsed Regime III [3], [11]. The changes in the injected current in each section produces changes of the local temperature by self-heating and cross-heating. In turn, these temperature changes result in changes in the refractive indices and therefore in the phase of the optical field. This effect gives rise to the quasi-periodic alternation of emission regimes. In addition, the carrier induced index changes when sweeping the injected currents also contribute to the complex dynamics of the device.

In the subsequent discussion, the competition between regimes will be interpreted as arising from longitudinal mode dynamics, i.e., not considering possible lateral multimode effects. This assumption is justified both, by the independence of the measured spectra on the position of the lensed fiber which collects only the light coming from a small region of the source, and also by the fact that 1-D simulation models [6]–[8], [11] were able to reproduce most of the emission regimes and wavelength jumps reported here.

The RF spectra in Figs. 3 and 4 are the most clear indicators of the different regimes: Regime I, absence of RF power; Regime II, RF peaks at 18 and 36 GHz; and Regime III, main RF peak at a variable frequency lower than 10 GHz. As mentioned in Section 3.1, regime I appears in three cases: i) low injection of the PA for the complete injection range of the MO (see Fig. 4, $I_{PA} = 1$ A); ii) high injection of the MO (see Fig. 3, $I_{MO} = 500$ mA), and iii) alternating with other regimes at intermediate injection conditions. In these conditions the gain provided by the PA is low, either because of the low injection in case i) or because of the carrier depletion when the optical power injected by the MO into the PA is high as in case ii). It is interesting to notice that in case i) the emission wavelength shifts continuously as a function of the MO current, while in cases ii) and iii) wavelength jumps occur. The occurrence of Regime II at low injection of the MO, and medium to high injection of the PA, alternating with Regime I will be explained later (see Fig. 3, $I_{MO} = 30$ mA).

The superlinear shift of the emission wavelength λ_{peak} as a function of the MO current shown in Fig. 4 for $I_{PA} = 1$ A is due to self-heating effects. In Fig. 6(a) we have plotted λ_{peak} as a function of the power dissipated in the MO section P_{dis}^{MO}, which can be estimated from $P_{dis}^{MO} = I_{MO} V_{MO}$

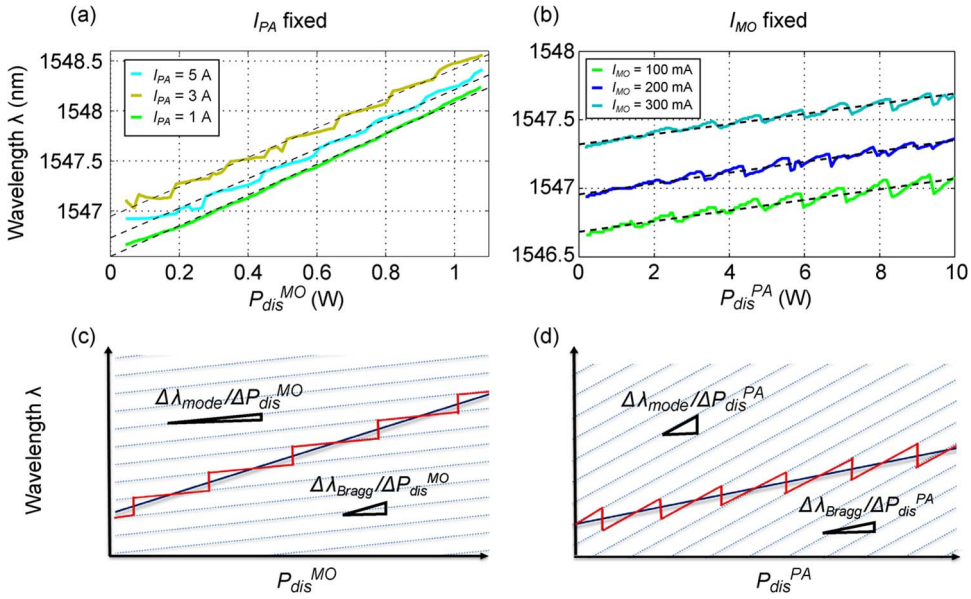

Fig. 6. (a) Emission wavelength as a function of $P_{\text{dis}}^{\text{MO}}$ (W) for $I_{\text{PA}} = 1, 3, 5$ A. (b) Emission wavelength as a function of $P_{\text{dis}}^{\text{PA}}$ (W) for $I_{\text{MO}} = 100$, 200, and 300 mA (the dashed lines show the linear trend). (c) Qualitative explanation of the wavelength evolution as function of $P_{\text{dis}}^{\text{MO}}$ for I_{PA} fixed and (d) as a function of $P_{\text{dis}}^{\text{PA}}$ for I_{MO} fixed.

when neglecting the power injected from the MO into the PA. A clear linear dependence with slope 1.6 nm/W is found. This linear dependence of λ_{peak} on $P_{\text{dis}}^{\text{MO}}$ is maintained in average for higher current in the PA (see Fig. 4), except for the appearance of quasi-periodical jumps towards longer wavelength. The precise height of the jumps is difficult to estimate but it ranges between 0.14 nm at low injection level to around 0.06 nm at high injection. In a similar way, Fig. 6(b) represents λ_{peak} vs. the power dissipated in the PA section $P_{\text{dis}}^{\text{PA}} = I_{\text{PA}} V_{\text{PA}} - P$.

As indicated by the dashed lines, the averaged shifts of λ_{peak} show again a linear dependence on $P_{\text{dis}}^{\text{PA}}$ for the whole set of I_{PA}. The slope is now 0.035 nm/W and again a smoother evolution of λ_{peak} is quasi-periodically interrupted by sudden drops. The two different dependencies of λ_{peak} on the dissipated powers (and therefore, on the currents in each section) shown Fig. 6(a) and (b) suggest a qualitative interpretation based on thermal effects. This is illustrated in Fig. 6(c) and (d).

In Regime I, for given bias conditions λ_{peak} depends on the refractive index of the DFB section through λ_{Bragg}, and also on the refractive index of the PA section due to the feedback at the front facet which contributes to the phase roundtrip condition of the lasing mode λ_{mode}. Neglecting the carrier effects on the refractive index, the variation of λ_{Bragg} with $P_{\text{dis}}^{\text{MO}}$ $(\Delta\lambda_{\text{Bragg}}/\Delta P_{\text{dis}}^{\text{MO}})$ will be much larger than the variation of λ_{Bragg} with $P_{\text{dis}}^{\text{PA}}$ $(\Delta\lambda_{\text{Bragg}}/\Delta P_{\text{dis}}^{\text{PA}})$, as the MO temperature will depend more on the self-heating than on the cross-heating. The opposite will be valid for λ_{mode}, with $\Delta\lambda_{\text{mode}}/\Delta P_{\text{dis}}^{\text{PA}}$ larger than $\Delta\lambda_{\text{mode}}/\Delta P_{\text{dis}}^{\text{MO}}$. Fig. 6(c) and (d) shows schematically the evolution of λ_{mode} and λ_{Bragg} with $P_{\text{dis}}^{\text{MO}}$ $(P_{\text{dis}}^{\text{PA}})$ according to previous considerations. The emission wavelength (red line) is that of the mode closest to λ_{Bragg}. This simple reasoning yields qualitatively the red (blue) wavelength jumps when sweeping I_{MO} (I_{PA}). The period of the wavelength jumps is then caused by the difference between slopes $\Delta\lambda_i/\Delta P_{\text{dis}}^{j}$ ($i =$ Bragg, mode; $j =$ MO, PA) In fact the period is closer to constant when plotting the wavelength vs the dissipated powers than when plotting vs the currents (compare Fig. 6(a) and (b) with Figs. 3 and 4), indicating the predominance of thermal over carrier effects. The origin of the wavelength separation between the modes, corresponding to the value of the jumps, is not clearly understood at the moment: we think that at low I_{MO} it corresponds to the FSR of the FP modes of the total cavity, but

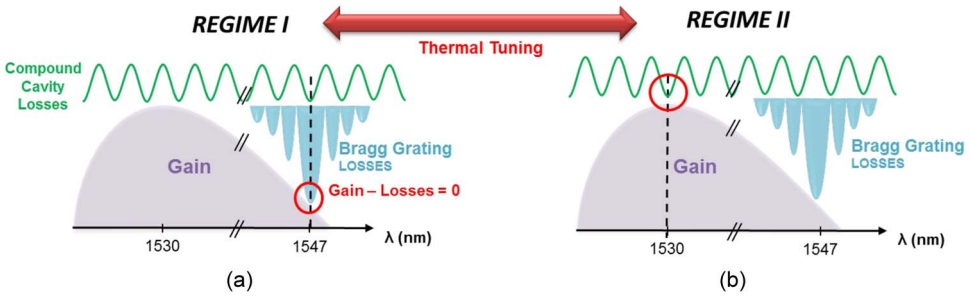

Fig. 7. Schematic representation of mode competition between compound cavity modes in the region of high material gain and the DFB peak. Thermal tuning shifts FP mode spectrum and originates quasi-periodic alternation between two different emission regimes: (a) Regime I: Emission at λ_{Bragg}. (b) Regime II: Emission at the gain peak.

that at higher MO current the active Bragg grating modifies the phase of the propagating field and reduces the mode spacing, as it has been observed theoretically and experimentally in [11]. Numerical modeling is in progress for a better understanding and confirmation of present interpretation.

The qualitative explanation of the mode competition (see Fig. 3) for $I_{MO} = 30$ mA between the FP modes of the total cavity (Regime II) and the DFB mode close to the Bragg wavelength (Regime I) is shown in Fig. 7. The FP mode losses are represented in green solid line, and the Bragg grating losses centered at the Bragg wavelength $\lambda \sim 1547$ nm are shown in blue. The gain spectrum shown in violet is centered according to the experiments around 1530 nm. The lasing condition is reached when the gain is equal to the total losses. In the ideal MOPA operation (regime I) this condition is reached at a wavelength close to the Bragg condition, as in DFB lasers [see Fig. 7(a)], but under slightly different driving conditions and due to the thermal tuning, the DFB mode losses decrease and the lasing condition reached at the center of the maximum gain. The thermal shift of the DFB mode when increasing the PA current induces the periodicity between emission regimes. The ripples in the $P - I_{PA}$ characteristics at low I_{MO} current are due to the transitions between emission regimes, with the peaks corresponding to Regime II and the valleys to Regime I.

The physical origin of the self-pulsed emission regime (Regime III) is difficult to be clearly determined. This regime appears with the same quasi-periodicity with the currents as the wavelength jumps and usually just before the jumps, but sometimes it appears inside a wavelength stable regime (see for instance the regime III region at $I_{MO} \sim 250$ mA in Fig. 4, $I_{PA} = 3$ A). The self-pulsation frequency increases as a function of I_{PA} and decreases as a function of I_{MO}. We think that the self-pulsations can be interpreted as undamped relaxation oscillations of the full cavity for particular values of the phase of the optical feedback. Further theoretical and experimental investigations are in progress for a better understanding of the complex dynamics of these devices.

5. Conclusion

We have characterized the emission properties of a monolithic high brightness 1.5 μm MOPA and have identified three quite different operation regimes: I, amplified DFB operation; II, multimode Fabry–Perot operation; and III, self-pulsed operation. Regime II takes place at low MO injection due to the residual reflectivity of the front facet and the large detuning between the Bragg grating and the maximum gain wavelength. Regime III seems to be a consequence of the phase of the active optical feedback which induces undamped relaxation oscillations. These regimes alternate quasi-periodically when changing the injected currents to the two sections. This alternation is attributed to the changes of the refractive index caused by self- and cross-heating which modify the coupling of the two optical cavities.

The detailed knowledge of the emission regimes allows the selection of appropriate operation points for different types of applications: either those requiring good spectral quality and high

power (Regime I) or those requiring the generation of high power RF signals in the GHz range (Regime III). Further experimental work is in progress to assess the suitability of these MOPAs for applications requiring a modulated high power beam.

References

[1] H. Wenzel *et al.*, "High peak power optical pulses generated with a monolithic master-oscillator power amplifier," *Opt. Lett.*, vol. 37, no. 11, pp. 1826–1828, Jun. 2012.

[2] P. Adamiec *et al.*, "High-peak-power pulse generation from a monolithic master oscillator power amplifier at 1.5 μm," *Appl. Opt.*, vol. 51, no. 30, pp. 7160–7164, Oct. 2012.

[3] M. W. Wright and D. J. Bossert, "Temporal dynamics and facet coating requirements of monolithic MOPA semiconductor lasers," *IEEE Photon. Technol. Lett.*, vol. 10, no. 4, pp. 504–506, Apr. 1998.

[4] A. Egan *et al.*, "Dynamic instabilities in master oscillator power amplifier semiconductor lasers," *IEEE J. Quantum Electron.*, vol. 34, no. 1, pp. 166–170, Jan. 1998.

[5] M. Spreemann, M. Lichtner, M. Radziunas, U. Bandelow, and H. Wenzel, "Measurement and simulation of distributed-feedback tapered master-oscillator power-amplifiers," *IEEE J. Quantum Electron.*, vol. 45, no. 6, pp. 609–616, Jun. 2009.

[6] S. Fürst, A. Perez-Serrano, A. Scire, M. Sorel, and S. Balle, "Modal structure, directional and wavelength jumps of integrated semiconductor ring lasers: Experiment and theory," *Appl. Phys. Lett.*, vol. 93, no. 25, Dec. 2008, Art. ID. 251109.

[7] P. M. Stolarz *et al.*, "Spectral dynamical behavior in passively mode-locked semiconductor lasers," *IEEE Photon. J.*, vol. 3, no. 6, pp. 1067–1082, Dec. 2011.

[8] M. Radziunas *et al.*, "Mode transitions in distributed-feedback tapered master-oscillator power amplifier: Theory and experiments," *Opt. Quantum Electron.*, vol. 40, no. 14/15, pp. 1103–1109, Nov. 2008.

[9] M. Vilera *et al.*, "Emission regimes in a distributed feedback tapered master-oscillator power-amplifier at 1.5 μm," in *Proc. SPIE*, 2014, vol. 9134, Art. ID. 91340N.

[10] K.-H. Hasler *et al.*, "5-W DBR tapered lasers emitting at 1060 nm with a narrow spectral linewidth and a nearly diffraction-limited beam quality," *IEEE Photon. Technol. Lett.* vol. 20, no. 19, pp. 1648–1650, Oct. 2008.

[11] S. Bauer *et al.*, "Nonlinear dynamics of semiconductor lasers with active optical feedback," *Phys. Rev. E*, vol. 69, no. 1, 2004, Art. ID. 016206.